RSC Advances

PAPER

View Article Online
View Journal | View Issue



Cite this: *RSC Adv.*, 2024, **14**, 22280

# Study on the occurrence state of main components of phosphogypsum dihydrate and its impurity distribution

Wanqiang Dong, [a] Ningjie Sun,[a] Xiangyi Deng,[a] Zhuo Chen,[a] Yuefei Zhang,[c] Ru'an Chi*[ab] and Lisong Hu[a]

The dihydrate phosphoric acid process is the mainstream technique. However, the phosphogypsum (PG) produced contains high levels of impurities such as phosphorus and fluorine, severely constraining its valorization. In order to elucidate the occurrence patterns of phosphorus and fluorine impurities in PG, this study employed analytical methods including XRF, XRD, AMICS (Automated Mineralogy Integrated with Chemistry System), XPS, and chemical element balance analysis. We investigated the occurrence states of phosphorus, fluorine, silicon, iron, and aluminum elements in PG from wet-process phosphoric acid production, as well as the distribution characteristics of phosphorus and fluorine impurities. Additionally, we utilized Density Functional Theory (DFT) calculations to determine the binding energies of major minerals with water-soluble phosphate and fluoride groups, and analyzed the zeta potentials of gypsum and quartz mineral surfaces. The results indicate that the main mineral phases in PG are gypsum, quartz, potassium silicate minerals, aluminosilicate minerals, and hematite, predominantly occurring in monomineralic forms. Phosphorus impurities primarily exist in calcium silicate and hematite minerals, while fluorine is mainly associated with gypsum and potassium silicate minerals. DFT calculations demonstrate strong binding energies between calcium silicate and hematite minerals with $PO_4^{3-}$, as well as between gypsum and quartz minerals with $F^-$. The acidic conditions in the separation tank during wet-process phosphoric acid production may contribute to the distinctive distribution characteristics of phosphorus and fluorine impurities in PG.

Received 3rd May 2024
Accepted 17th June 2024

DOI: 10.1039/d4ra03273j

rsc.li/rsc-advances



## 1. Introduction

Phosphorus is a non-renewable vital element and an economic mineral resource that is extensively utilized in various fields such as agriculture, chemical industry, pharmaceuticals, light industry, and national defence.[1–4] As of 2008, China has been the world's largest producer of phosphate rock, accounting for more than 50% of the world's total.[5] A huge industrial system has been formed for the development and utilization of phosphorus resources in China.[6] Wet process phosphoric acid (WPPA) plays a crucial role in the phosphorus chemical industry system. More than 90% of the total output of phosphate rock for WPPA is utilized for the production of phosphoric acid.[7,8] According to the various process streams, the WPPA process can be divided into the "dihydrate method", "hemihydrate method", and "dihydrate-hemihydrate method". The scope of operation and the range of process conditions of the "dihydrate method" are wider than the WPPA process based on the "dihydrate method" and "dihydrate-hemihydrate method", and its industrial application is also more extensive.[9–11] Based on incomplete statistics, the capacity ratio of WPPA factories in domestic production using the "dihydrate method" reaches about eighty percent.[12,13] However, it should be emphasized that compared to the WPPA "hemihydrate method" and "dihydrate-hemihydrate method", the "dihydrate method" process produces phosphogypsum (PG) with a higher impurity content, in which the $P_2O_5$ content is about 1.7%, and the water-soluble fluorine reaches 1.12%.[14] The water-soluble phosphorus in PG reduces the dehydration activation energy of $CaSO_4\ 2H_2O$ in PG, which leads to an increase in setting time and a decrease in the mechanical strength of PG-based gypsum products. After the formation of $CaF_2$ from F dissolved in PG, the hydration process of PG-based materials is delayed, resulting in the deterioration of its initial physical and mechanical properties, the continuous leaching of phosphorus and fluorine impurities from PG when used as a cementitious material for mine backfill may lead to new environmental pollution issues.[15,16] To some extent, this also limits the large-scale use of phosphogypsum-based cementitious materials,and severe limitations caused by phosphorus and fluorine impurities in PG against the comprehensive utilization of PG resources.[17,18]

[a]*School of Resources and Safety Engineering, Wuhan Institute of Technology, Wuhan 430205, Hubei, China*

[b]*Hubei Three Gorges Laboratory, Yichang 430073, Hubei, China*

[c]*School of Chemistry and Enviromental Engineering, Wuhan Institute of Technology, Wuhan 430205, Hubei, China. E-mail: rac@wit.edu.cn*

The middle and lower reaches of the Yangtze River represent significant bases for the exploitation of phosphate rock resources and phosphorus chemical industries in China. 80% of phosphate rock resources and 65% of phosphorus chemical industries are distributed in the Yangtze River Basin.[19] Therefore, the middle and lower reaches of the Yangtze River are also the main areas of PG production. In 2021, the production of PG in Hubei province alone was up to 30 million tons.[20,21] PG storage occupies a lot of land resources and easily causes environmental pollution.[22] The only way to realize the sustainable development of phosphorus chemical industries is to realize the harmless disposal of PG and further improve the level of comprehensive utilization.[23,24] Up till now, scientific researchers have conducted a lot of research on improving the harmless disposal source of PG and optimizing the process to improve the quality of PG. A research achievement, using silicon powder (SP) to enhance the fluorine recovery during the WPPA concentration process, has realized the reduction of fluorine deposit formation during the WPPA concentration process[25] Modified spirulina-activated bentonite (MSAB) was employed as an adsorbent to adsorb and purify uranium, nickel, lead, and other metal ion impurities present in the ionic state in WPPA, which met the source improvement of WPPA.[26] Researchers have employed the ozone–hydrogen–peroxide advanced oxidation process to enhance the acidolysis process of phosphate rock.[27] The results revealed that the acidolysis reaction of apatite ore in the WPPA process incorporates the reduction of the impurity phosphorus content in PG from the source. Although the raw material upgrading and the process strengthening approaches currently used can achieve the purification of PG produced by the WPPA to some extent, with the continuous decline of domestic phosphate rock quality, it is commonly difficult to guarantee the quality of PG produced from the source. An in-depth investigation of the occurrence characteristics of impurities in PG to develop a deep purification process is one of the feasible ways to comprehend the utilization of PG resources.[28]

PG has mineralogical characteristics, and mineral processing technology can be effectively employed for deep purification of PG, however, the impurities in PG are complex. In addition to soluble phosphorus and fluorine impurities with strong migration, there are also oxide impurities and organic substances such as silicon, iron, and aluminum. In recent years, existing research has focused on the removal of soluble phosphorus and fluorine impurities in PG. Insufficient investigation on the occurrence law of impurities in PG, including fluorine, iron, aluminum, and silicon, and the lack of process mineralogical data seriously have restricted the exploitation of high-value resources in PG.[29–32] Herein, the mineral phase composition of the main impurities of PG and the distribution characteristics of phosphorus and fluorine impurities in PG are methodically examined by using process mineralogy and chemical element balance analysis. The density functional theory (DFT) and the binding energies of the main mineral phases in PG such as gypsum and quartz minerals as well as $PO_4^{3-}$ and $F^-$ were appropriately evaluated.[33,34] The study utilizes these findings to investigate the distribution patterns of phosphorus and fluorine impurities in PG. This is carefully performed by analyzing the variation of zeta potential in relation to the pH value on the surface of gypsum and quartz minerals. In addition, solidification experiments using calcium oxide as a curing agent were conducted to verify the occurrence states of phosphorus and fluorine impurities in phosphogypsum. The findings of this paper are expected to provide theoretical guidance for the source improvement of PG in the WPA production process and the efficient solidification of phosphorus and fluorine impurities in the harmless disposal of PG.

## 2. Experimental study

### 2.1. Reagents and instruments

The reagents used in the experiment were dihydrate PG obtained from the "dihydrate method" in a phosphate fertilizer production enterprise in Yichang. $HNO_3$ and NaOH used for pH adjustment were purchased from Sinopharm and both were analytically pure. The surface morphology of PG was carefully examined by Tescan Vega 3 scanning electron microscope (SEM). Additionally, the mineral phase composition of PG was analyzed by XRD-6000 diffractometer, the mineral surface potential was measured by Zetasizer Nano potential analyzer, and the XPS analysis was carried out by Thermo Scientific K-Alpha type X-ray electron spectrometer.

### 2.2. Experimental method

The PG samples were mixed and reduced, and the chemical elements of the reduction samples were analyzed. The microstructure and surface element composition of PG crystals were analyzed *via* scanning electron microscopy and energy spectrum analysis (SEM-EDS). The distribution ratio of impurity elements in PG in various mineral phases was determined by AMICS (Automatic Mineral Identification and Characterization System). Based on the chemical element equilibrium analysis, the characteristics and occurrence mechanisms of impurity elements (mainly including phosphorus, fluorine, silicon, iron, aluminum, and potassium) in PG were investigated. The mineral surface was analyzed by a Thermo Scientific K-Alpha X-ray electron spectrometer and calibrated based on the C 1s spectrum of 284.80 eV. The data were then appropriately fitted by Avantage software to analyze the chemical element composition and chemical bonding form of the PG surface.

### 2.3. DFT calculation simulation

In this paper, the first principle thinking software VASP is employed to calculate the binding energy between the main

Table 1 Chemical composition and content of PG

| | |
|---|---|
| Calculation Task | Geometric optimization |
| Calculation accuracy | Fine |
| Optimization method | Conjugate gradient algorithms |
| Exchange correlation | GGA-PBE |
| Energy cut-off | 450 eV |
| Iterative convergence criteria | $10^{-5}$ eV |
| Atomic force convergence criteria | 0.01 eV Å |
| Pseudopotential | PAW |

mineral phases and $PO_4^{3-}$ and $F^-$ in PG. The exchange correlation is based on the generalized gradient approximation (GGA) and the PBE functional.[35] The energy cutoff used to extend the Kohn–Sham electron wave function is set equal to 400 eV. The energy criterion for iterative convergence is also set as $10^{-5}$. Let us relax all atoms in the model so that the Hellmann–Feynman force is less than 0.01 eV $Å^{-1}$. The main calculation parameters and convergence conditions are provided in Table 1.

## 3. Analysis and discussion of the experimental results

### 3.1. Sample analysis

**3.1.1. Analysis of the chemical composition and microscopic morphology.** The PG used in this experiment was obtained from a WPPA plant in Yichang, Hubei Province, does not possess radioactivity. The chemical composition of PG was investigated using X-ray fluorescence spectrometry (XRF), and the obtained results are provided in Table 2. As is seen, the impurities in PG are mainly Si, P, F, K, Al, and Fe, and the content of non-metallic impurities such as Si, P, and F is substantially higher than metallic impurities such as K, Al, and Fe. Fig. 1 illustrates the SEM-EDS image of a rhombic tabular PG crystal. The results indicated that the crystallinity of calcium sulfate crystal in PG was good when it was grown along (020) planes and the crystal planes were easily disturbed by impurities during the crystal growth process.[36] It is generally believed that tabular and short rod PG crystals form under good crystal growth conditions. The scan mapping results reveal that the $CaSO_4\ 2H_2O$ crystal growth in the WPPA process still has a large number of impurities under ideal conditions. Fig. 1 shows the surface scanning results of the main chemical elements in phosphogypsum. As illustrated, the contents of Ca, S, and P in phosphogypsum are significantly higher than those of other elements. Elements such as P, F, Si, Al, K, and Fe are clearly enriched in some regions.

**3.1.2. Mineral phase analysis of PG.** Sample phase analysis is shown in Fig. 2. The spectrum of XRD analysis shows that the main mineral phases in PG are gypsum, quartz, and fluorapatite

Table 2 Results of the chemical multielement analysis of PG (%)

| Element | $SO_3$ | CaO | $SiO_2$ | $P_2O_5$ | F | $K_2O$ | $Al_2O_3$ | $Fe_2O_3$ | BaO | $TiO_2$ | SrO |
|---|---|---|---|---|---|---|---|---|---|---|---|
| Mass fraction/% | 52.63 | 32.70 | 10.38 | 1.72 | 1.12 | 0.58 | 0.50 | 0.34 | 0.15 | 0.10 | 0.05 |

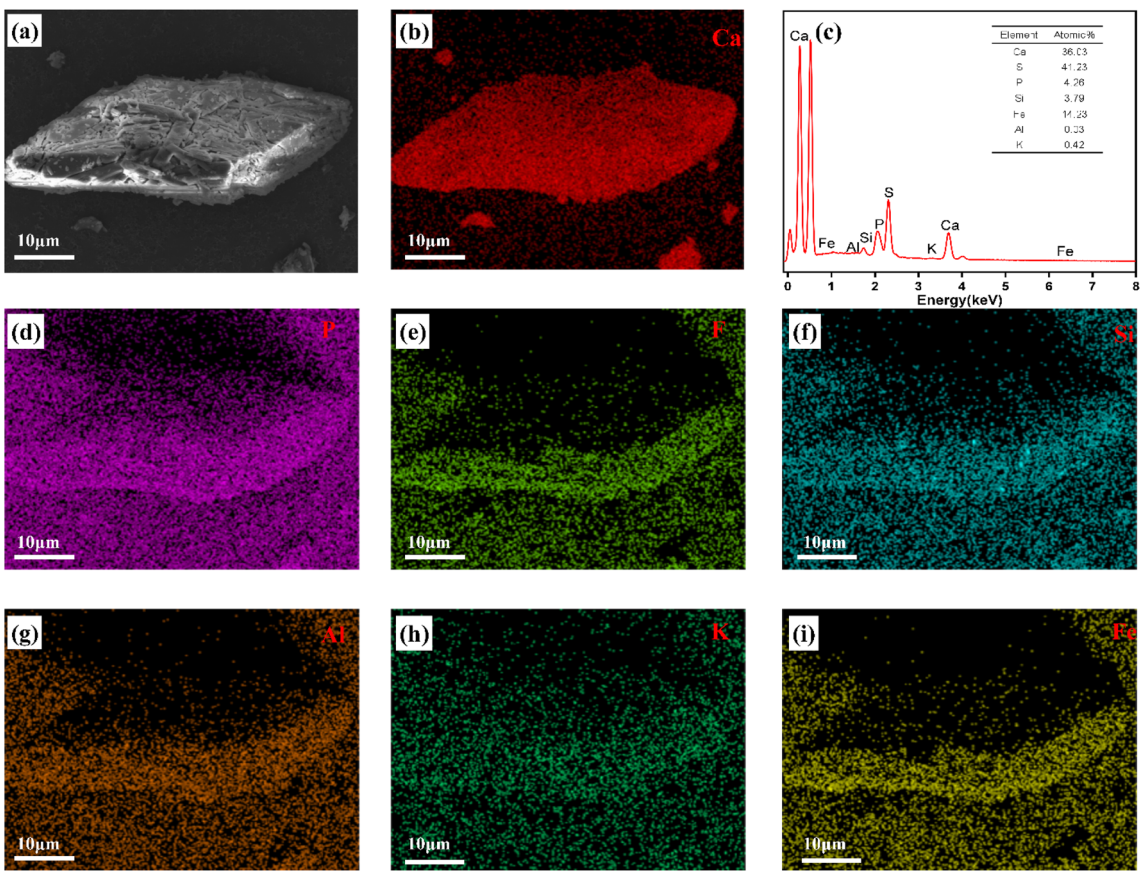


Fig. 1 SEM-mapping scanning results of PG.

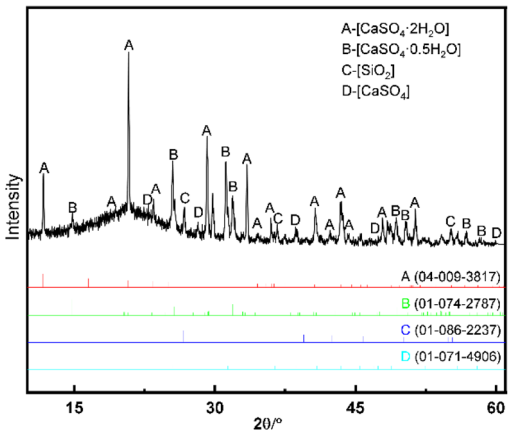


Fig. 2 XRD analysis results of PG.

minerals and the absorption peak is a strong characteristic of gypsum absorption peak. The characteristic absorption peaks of quartz and fluorapatite were partially covered by the strong absorption peak of gypsum, indicating that the mineral phase content of gypsum in PG was high and crystallinity was good. The results of the chemical multi-element analysis show that there are mineral phases containing iron, aluminum, and other impurities in PG, but due to the low content, it was difficult to analyze it by the XRD method, so it needed to be analyzed *via* other test methods. The composition and content of the mineral phase in PG were investigated based on the XRD analysis, and the content of the main mineral phase in PG was calculated by semi-quantitative analysis method. However, it is worth noting that the semi-quantitative XRD analysis approach makes it difficult to determine the mineral phase with relatively low content in the mineral and cannot be used to determine the intergrowth and symbiotic relationship among different mineral phases. Therefore, it is necessary to explore the distribution characteristics among various minerals in PG with the help of other characterization analysis approaches.

### 3.2. Analysis of the mineral liberation degree of PG

The composition of mineral species directly affects the occurrence characteristics of elements in minerals.[37,38] PG presents mineralogical characteristics. Except for water-soluble phosphorus and fluorine, other impurity elements mainly exist in the form of mineral phases in PG. In this article, the degree of release and intergrowth relationship of the main mineral phases in PG are also of concern. The distribution characteristics of the main impurity elements in PG can be determined by combining the chemical composition of the mineral phases. For this purpose, PG was analyzed using an automatic mineral analysis system, and the liberation degree of gypsum, quartz, potassium silicate, calcium aluminate, rutile, biotite, pyrite, chlorite, and wollastonite monomer, as well as the intergrowth and symbiotic relationship among minerals were determined. According to the analysis results in Table 3, the mineral phases in PG are mainly in the form of monomer minerals, and the distribution ratios of gypsum and quartz monomers in order are 92.18 and 80.84%. The proportions of occurrence and distribution of potassium silicate, calcium aluminate, rutile, biotite, pyrite, chlorite, and wollastonite in PG are 81.62%, 96.51%, 96.63%, 89.30%, 76.59%, 87.45%, and 85.84%, respectively. It is worth mentioning that calcium aluminate and rutile were almost all in the form of monomer minerals. The intergrowth degrees of potassium silicate, calcium aluminate, rutile, biotite, pyrite, chlorite, wollastonite, and gypsum minerals were evident as 0.32%, 0.77%, 0.04%, 3.86%, 0.00%, 0.83%, and 0.44%, indicating an obvious intergrowth relationship between gypsum and minerals including potassium silicate, calcium aluminate, biotite, and wollastonite. The intergrowth degrees of potassium silicate, calcium aluminate, rutile, biotite, pyrite, chlorite, wollastonite, and quartz minerals were obtained as 0.00%, 0.00%, 0.95%, 0.40%, 7.56%, 2.13%, and 0.15%, respectively, indicating that a significant intergrowth relationship of quartz minerals with rutile, biotite, pyrite, and chlorite.

According to Ennaciri *et al.*[37] the occurrence of phosphorus, fluorine, and iron impurity elements in PG is closely related to the characteristic impurity mineral components. The contents of gypsum, quartz, potassium silicate, calcium silicate, rutile, and biotite in the PG samples used in this study in order are 82.58, 8.73, 1.64, 0.62, 0.41 and 0.30%. The minerals produced in the form of monomer minerals constitute 85.70% of the total mass of PG. Therefore, the dissociation degree relationship of mineral phases in PG provides basic data to analyze the distribution characteristics of impurity elements in various mineral phases.

### 3.3. Study on the occurrence characteristics of the main impurity elements in PG

**3.3.1. Spectroscopic analysis of the element occurrence state.** The chemical element state and composition of the PG surface were analyzed by XPS technology. As demonstrated in Fig. 3(a), some characteristic peaks were detected at 75.15 eV, 103.6 eV, 134.23 eV, 169.28 eV, 248.8 eV, 348.08 eV, 458.88 eV, 532.19 eV, and 711.18 eV in the XPS full spectrum of PG, corresponding to the elements Al 2p, Si 2p, P 2p, S 2p, C 1s, Ca 2p, Ti 2p, O 1s, and Fe 2p, respectively. As demonstrated in Fig. 3(b), the C1s high-resolution spectrum was split and fitted into three peaks at 284.7 eV, 285.34 eV, and 286.1 eV, corresponding to C–C/C=C, C–O, and C=O bonds, respectively. The high-resolution XPS P 2p spectrum is illustrated in Fig. 3(c). It can be seen that the spectral signal is divided and fits into two peaks. The two characteristic peaks of $PO_4^{3-}$ at 134.03 eV and 134.93 eV correspond to P $2p^{3/2}$ and P $2p^{1/2}$. Relevant studies indicate that in the binding energy range of 130.9–136 eV, phosphorus oxides may be in a P–N or P–O environment. The XRF multi-element analysis results of the test samples did not detect the presence of nitrogen, so it can be determined that this is a P–O environment.[39,40] According to the statistical research by Kim S. Siow *et al.*,[41] phosphorus oxides in the form of $PO_4^{3-}$ have a binding energy of around 134.0 eV. Therefore, it can be further confirmed that phosphorus in phosphogypsum mainly exists in the form of $PO_4^{3-}$. The high-resolution XPS F 1s

Table 3 Results of the chemical multielement analysis of PG (%)

| | | Connectivity/% | | | | | |
|---|---|---|---|---|---|---|---|
| Mineral | Monomer | Quartz | Biotite | Calcium aluminate | Potassium silicate | Pore | Other minerals |
| Gypsum | 92.18 | 0.01 | 0.02 | 0.01 | 0.01 | 4.47 | 3.30 |

| | | Connectivity/% | | | | |
|---|---|---|---|---|---|---|
| Mineral | Monomer | Gypsum | Rutile | Pyrite | Pore | Other minerals |
| Quartz | 80.84 | 0.11 | 0.09 | 0.21 | 15.09 | 18.74 |

| | | Connectivity/% | | | | |
|---|---|---|---|---|---|---|
| Mineral | Monomer | Wollastonite | Gypsum | Biotite | Pore | Other minerals |
| Potassium silicate | 12.40 | 81.62 | 0.34 | 0.32 | 0.08 | 5.24 |

| | | Connectivity/% | | | | |
|---|---|---|---|---|---|---|
| Mineral | Monomer | Fluorapatite | Gypsum | Rutile | Pore | Other minerals |
| Calcium aluminate | 96.51 | 0.02 | 0.77 | 0.06 | 2.48 | 0.16 |

| | | Connectivity/% | | | | |
|---|---|---|---|---|---|---|
| Mineral | Monomer | Quartz | Gypsum | Calcium aluminate | Pore | Other minerals |
| Rutile | 96.63 | 0.95 | 0.04 | 0.09 | 2.12 | 0.17 |

| | | Connectivity/% | | | | | |
|---|---|---|---|---|---|---|---|
| Mineral | Monomer | Quartz | Gypsum | Calcium iron olivine | Potassium silicate | Pore | Other minerals |
| Biotite | 89.3 | 0.4 | 3.86 | 0.37 | 0.38 | 3.15 | 2.54 |

| | | Connectivity/% | | |
|---|---|---|---|---|
| Mineral | Monomer | Quartz | Pore | Other minerals |
| Pyrite | 76.59 | 7.56 | 5.59 | 10.25 |

| | | Connectivity/% | | | |
|---|---|---|---|---|---|
| Mineral | Monomer | Quartz | Gypsum | Pore | Other minerals |
| Chlorite | 87.45 | 2.13 | 0.83 | 7.82 | 1.77 |

| | | Connectivity/% | | | | | |
|---|---|---|---|---|---|---|---|
| Mineral | Monomer | Quartz | Gypsum | Calcite | Potassium silicate | Pore | Other minerals |
| Wollastonite | 85.84 | 0.15 | 0.44 | 1.01 | 2.45 | 7.08 | 3.03 |

spectrum has been illustrated in Fig. 3(d). The plotted results reveal that the spectral signal can be divided and fitted into two peaks. The two characteristic peaks of F at 685.44 eV and 687.34 eV correspond to the characteristic peaks of chemical bonding of metal fluoride and organic fluoride, respectively. From the mineralogical analysis results, it can be determined that the two characteristic peaks of F were Ca–F and Si–F chemical bonds, respectively, which indicates that F is mainly present in the form of metal fluoride salts in PG, which accounts for about 69.48%. The high-resolution XPS spectrum of Si 2p has been presented in Fig. 3(e). The results indicate that the spectral signal can be split and fitted into three peaks, which are located in three characteristic peaks of 102.40 eV, 103.46 eV, and 104.04 eV. Among them, 102.40 eV corresponds to the

 

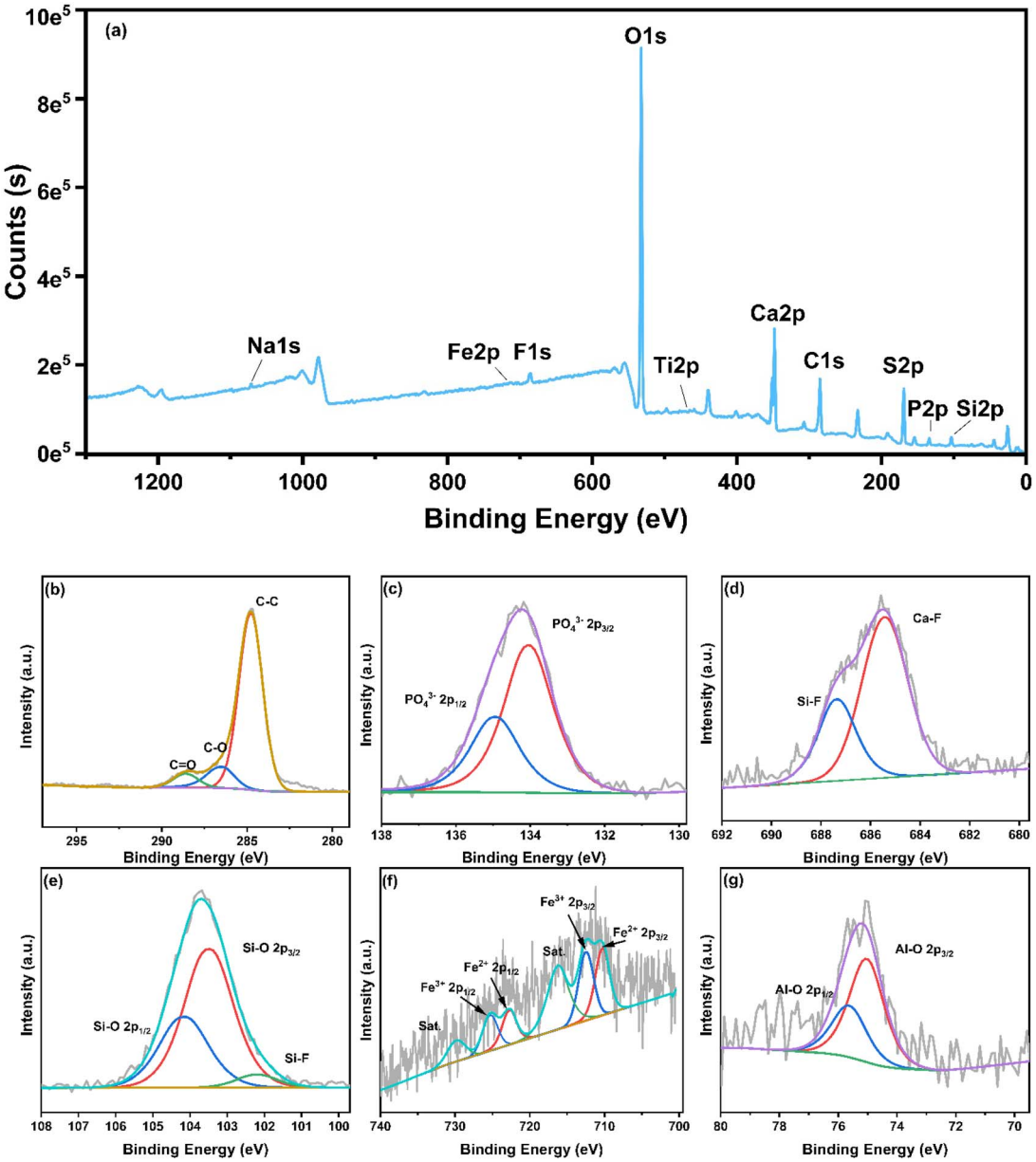


Fig. 3 Spectroscopic analysis results of the occurrence state of the PG: (a) total spectrum, (b) C, (c) P, (d) F, (e) Si, (f) Fe, (g) Al.

characteristic peak of aluminosilicate minerals, 103.46 eV and 104.04 eV in order correspond to the $2p^{3/2}$ and Si $2p^{1/2}$ Si–O bond states. This confirms that Si is essentially produced in the form of quartz minerals to a certain extent. As shown in the high-resolution spectrum of Fe 2p in Fig. 3(f), the two characteristic peaks of $Fe_3O_4$ at 710.2 eV and 712.47 eV in order correspond to Fe $2p^{3/2}$ and Fe $2p^{1/2}$, indicating the presence of $Fe^{2+}$ and $Fe^{3+}$ ions to a certain extent. In addition, the $Fe^{2+}$ satellite peaks at 716.23 and 725.30 and those of $Fe^{3+}$ at 722.66 and 729.84 eV further indicate that Fe exists in PG as $Fe^{2+}$ and $Fe^{3+}$. Kazragis believed that insoluble $FePO_4$ and soluble ferric sulfate would be produced in the WPA process.[42] At the same time, according to the static leaching test analysis of the experimental sample, in the case of pH > 4, Fe is almost insoluble, so we believe that Fe in the PG sample is mainly present in the form of insoluble compounds. The XPS spectrum of Al 2p has been demonstrated in Fig. 3(g) which exhibits two peaks at 75.02 eV and 75.62 eV. These represent characteristic peaks pertinent to the Al–O bond and suggest that the aluminum element is mainly present in the form of aluminosilicate in the analysis of PG. Based on the above results, analysis of Si 2p spectrum at 103.6 eV and F 1s spectrum at 685.44 eV reveals that F in PG exists mainly in the form of metal fluoride followed by fluosilicate. Additionally, analysis of the P 2p spectrum is indicative of the fact that phosphorus in PG is mostly present in the form of $PO_4^{3-}$, but the main mineral phase of occurrence could not be determined.

**3.3.2. Analysis of the element distribution characteristics.** The impurity mineral phase in PG is relatively complex. The content of the target elements and the type of mineral phase of

the main impurity in PG is determined by XRF analysis and XRD analysis, but the occurrence characteristics of the target impurity elements in different mineral phases of PG are not known. To investigate the distribution characteristics of various impurity elements in related mineral phases, element balance analysis was performed based on the mineral content (Fig. 4) of the sample and the distribution ratio of P, F, Si, Fe, Al, K, and other elements in PG in related minerals. The corresponding analysis results are presented in Fig. 4 and 5. As is seen, element P is mainly present in calcium silicate minerals, rutile, wollastonite, and fluorapatite with distribution ratios of 50.45, 19.46, 9.08%, and 9.69%, respectively. The phosphorus element in fluorapatite is mostly insoluble, and soluble phosphorus may exist mainly in calcium silicate and rutile mineral phases. In combination with the above XPS analysis results, the obtained results reveal that the phosphorus element in PG is mainly in the form of $PO_4^{3-}$ and there is almost no phosphorus-containing component in the pure mineral phases of calcium silicate and rutile. Therefore, there may be chemisorption among the water-soluble phosphoric acid component, calcium silicate, and rutile, which then leads to the enrichment of phosphorus elements in the calcium silicate and rutile. F mainly exists in gypsum, potassium silicate, and calcium aluminate minerals with distribution ratios of 73.94, 15.52, and 3.97%, respectively. Fluorine element is mostly insoluble in potassium silicate and calcium aluminate minerals, and the typical mineral is potassium fluosilicate, soluble fluorine may exist mainly in the gypsum mineral phase. The results of XPS analysis show that the content of F in PG in the form of metal fluoride is 69.48%, which is equivalent to the distribution rate of F in gypsum obtained from process mineralogical analysis. Relevant investigations have revealed that when the pH value in the system is more than 2.0, $F^-$ reacts with $Ca^{2+}$ and forms $CaF_2$ precipitation. Considering that the pH value of the system in the acidolysis and filtration processes of the WPA system is less than 2, we believe that the fluorine-containing substances in the form of metallic fluoride in gypsum are mainly soluble fluoride salts such as KF and NaF. In this form, F possesses a strong migration ability, and Fe is mainly present in pyrite, quartz, biotite, iron olivine, and magnetite, and their distribution ratios are obtained as 35.94, 21.53, 12.27, 6.20, and 9.37%, respectively, which are associated with the insoluble mineral phases. Al element mainly exists in quartz, calcium aluminate, chlorite, biotite, and anorthite minerals with distribution ratios of 29.38, 26.15, 14.68, 12.00, and 5.12%, respectively. K element is mainly found in potassium silicate minerals, quartz, and biotite with a distribution ratio of 86.27% in potassium silicate. Additionally, according to the element balance analysis, the concentration of element P in calcium silicate and rutile of PG is significantly higher compared to other components. Element F, on the other hand, is enriched in the mineral phase of gypsum, whereas element K is predominantly present as potassium fluosilicate. Furthermore, Fe and Al elements in PG do not exhibit substantial enrichment characteristics.

### 3.4. Analysis of distribution characteristics mechanism of phosphorus and fluorine impurities

The adsorption mechanism of a specific type of substance on a specific material can be simulated by density functional theory (DFT). The phosphorus and fluorine impurities in PG exhibit significant distribution characteristics in various minerals. To clarify the direct interaction mechanism between phosphorus and fluorine impurities in PG and different minerals, binding energies of main mineral phases and $PO_4^{3-}$ and $F^-$ in PG are calculated in this paper. The main calculation parameters and convergence conditions are provided in Table 1. The calculation results reveal that under ideal conditions, the binding energies of quartz, gypsum, potassium silicate, calcium silicate, and rutile

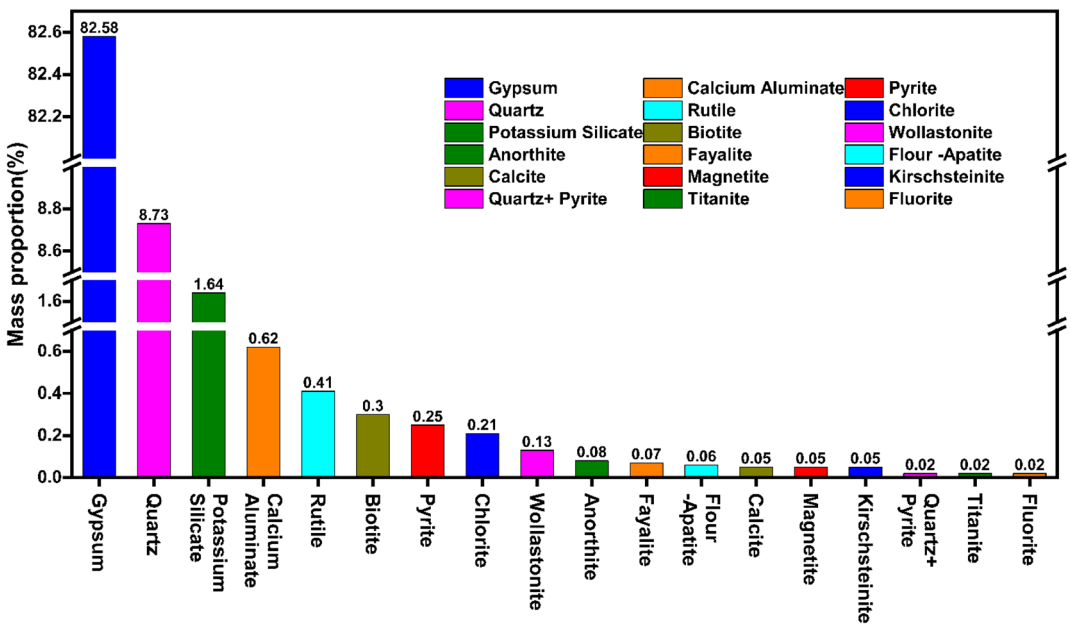


Fig. 4 Mass proportion of the main mineral phases in PG.

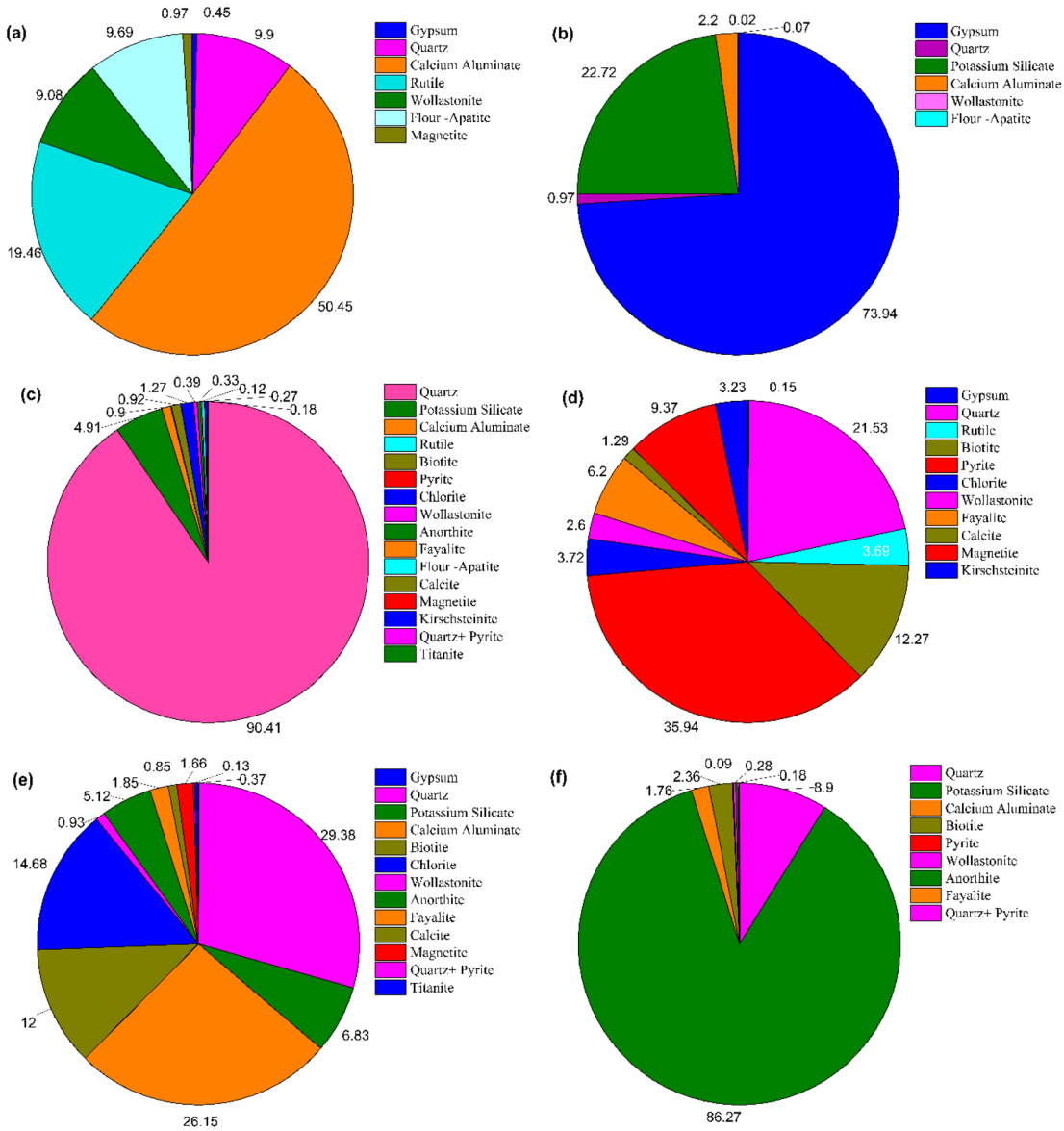


Fig. 5 Distribution ratio of the main impurity elements in PG in various mineral phases: (a) P, (b) F, (c) Si, (d) Fe, (e) Al, (f) K.

with $PO_4^{3-}$ and $F^-$ are less than zero, which indicates that these five mineral phases have a strong binding ability with $PO_4^{3-}$ and $F^-$. Further, the binding energy of $PO_4^{3-}$ with calcium silicate and rutile is substantially lower than that of $PO_4^{3-}$ with the other three minerals, indicating that $PO_4^{3-}$ binds more easily with calcium silicate and rutile. The binding energy of $F^-$ with gypsum and quartz is significantly lower than the binding energies of $F^-$ with potassium silicate, calcium silicate, and rutile minerals. As a result, $F^-$ tends to be enriched in gypsum and quartz minerals. The DFT calculation results are indicative of the fact that the enrichment rule of $F^-$ in gypsum minerals, but the results obtained from the process mineralogical analysis show that $PO_4^{3-}$ is only enriched in calcium aluminate and rutile. In addition, such results indicate that the distribution of $PO_4^{3-}$ in gypsum was only 0.45% and that of $PO_4^{3-}$ in quartz increased to 9.9%. Both gypsum and quartz crystal surfaces in phosphogypsum contain a large number of oxygen atoms. In a weakly acidic environment, the electrokinetic potential on the mineral surface is less than 0. At this point, there are many negatively charged oxygen atoms on the mineral surface, significantly reducing the electrostatic adsorption capacity between the mineral particles and $F^-$ and $PO_4^{3-}$.[43,44] During the production of WPA, the pH value of the acidolysis tank was less than 1, and the filter tank of the phosphoric acid and PG separation section had a pH value of 1–2 in operational conditions. The operating conditions of the WPA acidolysis reaction tank and the filter tank were strong acidic environments with pH $\leq$ 2. This paper measured the zeta potential on the surfaces of gypsum and quartz minerals under pH conditions of 0–6, as the test results illustrated in Fig. 7. From the results of the zeta potential test, it can be seen that in the case of pH $\leq$ 1, the surfaces of gypsum and quartz mineral particles have electropositivity. Additionally,

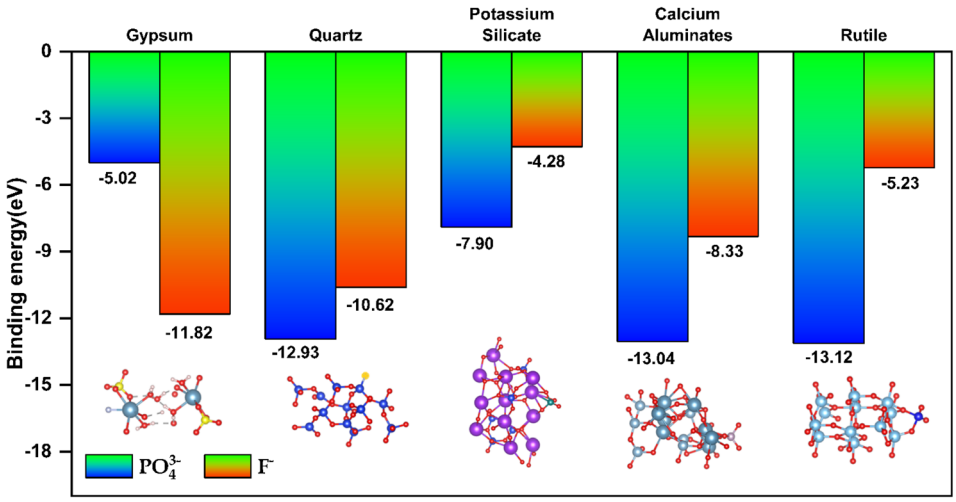


Fig. 6 Binding energy values among the main mineral phases and phosphorus and fluorine.

in the case of pH = 2, the surface of quartz mineral particles still presented electropositivity, while the eta potential value of gypsum was less than zero. Under such conditions, quartz and $PO_4^{3-}$ groups would be prone to electrophilic adsorption, so the distribution of $PO_4^{3-}$ in quartz was significantly higher than that of gypsum. Additionally, the DFT calculation results are consistent with the results obtained from the element equilibrium analysis (Fig. 6).

### 3.5. PG solidification test

According to XPS analysis, fluorine in PG exists in the form of alkali metal fluorine salt. Combined with the distribution characteristics of phosphorus and fluorine impurities and the DFT binding energy calculation results, it can be seen that $PO_4^{3-}$ in PG is mainly present in the form of water-soluble phosphate, which has a strong migration ability. Therefore, for the disposal of PG by the stacking method, the appropriate curing agent can be selected to effectively cure the impurities of phosphorus and fluorine dissolved in water in PG to realize the harmless disposal of PG. In this article, CaO powder has been utilized as a curing agent. For 3.0% CaO powder under the curing temperature of 30 °C for 150 minutes, the curing rate of water-soluble phosphorus in PG reached 98.5%, and the curing rate of water-soluble fluorine impurities was obtained more than 99.0%. The SEM-EDS analysis results of PG samples after the curing process have been illustrated in Fig. 8. The SEM micrograph demonstrates that loose flocculent deposits are formed on the surface of the cured PG particles. The energy spectrum analysis results indicate that the cured PG has a significantly increased F atom content from 0.09% to 16.78% and P atom content from 4.26% to 5.02% compared to the original PG. This suggests that during the calcination process, the fluoride in the alkali metal fluoride salt mainly solidifies with $CaF_2$ as the primary precipitation product. According to the analysis results, the water-soluble fluoride in PG primarily exists on the surface of PG minerals in the form of alkali metal fluoride salt. Its ability to move around is considerably higher than that of the water-soluble

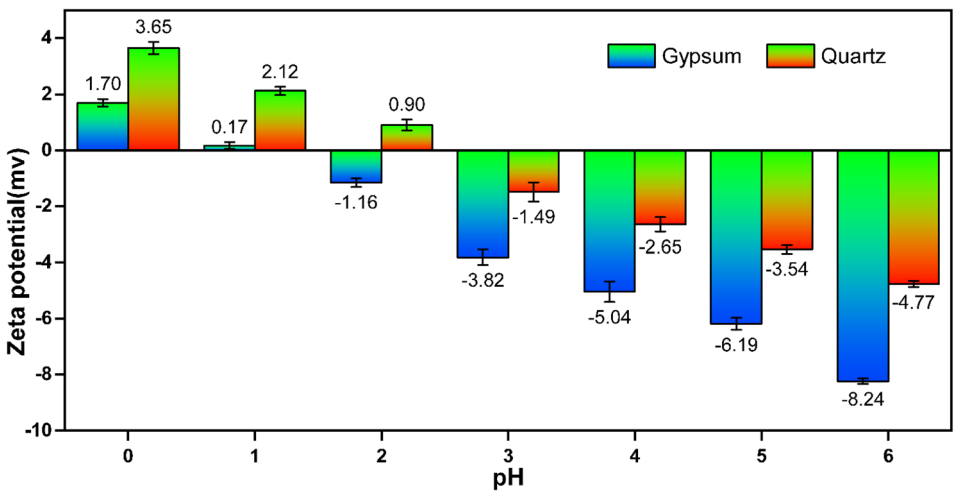


Fig. 7 Zeta potential analysis results of gypsum and quartz.

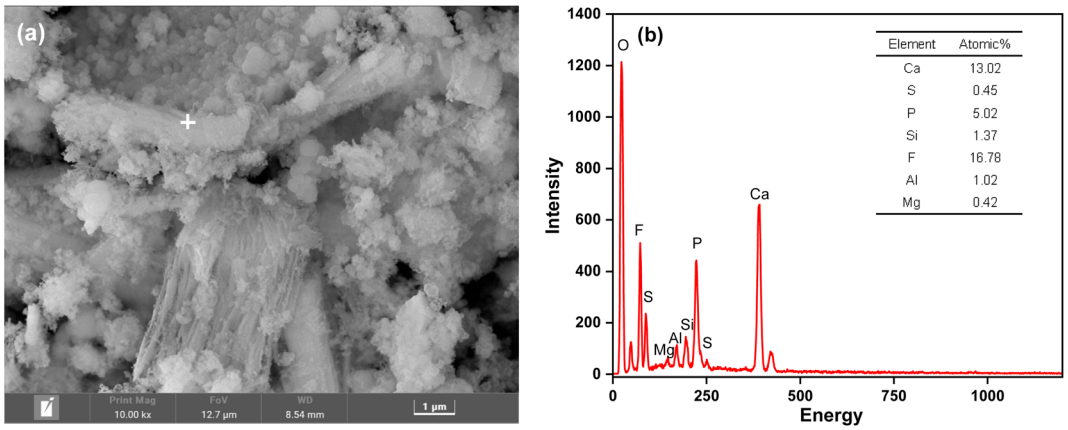


Fig. 8 SEM-EDS analysis results of the PG samples after the curing process: (a) SEM, (b) EDS.

phosphorus in PG. Therefore, it is a significant pollutant that should be prioritized in the environmental risk analysis of PG.

## 4. Conclusions

(1) The process mineralogical analysis reveals that gypsum has a significant intergrowth relationship with potassium silicate, calcium aluminate, biotite, and wollastonite, while quartz minerals exhibit a significant intergrowth relationship with rutile, biotite, pyrite, and chlorite. The distribution of phosphorus impurities in calcium aluminate and rutile is remarkably higher than the average. The distribution ratio of fluorine impurities in gypsum is obtained up to 73.94%. The distribution of iron impurities in the impurity mineral phase was relatively balanced, and the distribution of aluminum impurities in quartz and calcium aluminate was significantly higher than in other components. The results of XPS valence analysis indicate that phosphorus is mainly present in the form of $PO_4^{3-}$ in PG, while fluorine mainly exists in the form of metal fluoride salt in PG, followed by fluoride, Fe element mainly exists in insoluble form, and K element mainly occurs in potassium silicate mineral.

(2) The results of the balance analysis of chemical elements show that phosphoric acid is enriched in the mineral phase of calcium aluminate and rutile, as well as fluorine within gypsum and potassium silicate minerals, which demonstrates significant enrichment and distribution characteristics. The results of DFT calculations reveal that the binding energy between phosphate and calcium aluminate and rutile is significantly higher than that and other minerals. In addition, the binding energies among the fluoride, quartz, and potassium silicate minerals are significantly higher than in other cases. In the production process of WPPA, $PO_4^{3-}$ most likely had an electrophilic adsorption reaction with quartz under the operating conditions of pH $\approx$ 2 in the filter tank, which may be the main reason for the distribution characteristics of phosphorus and fluorine impurities in PG.

(3) In the harmless treatment of PG *via* the curing method, the use of a curing agent to neutralize the acidity of PG is able to achieve efficient curing of water-soluble phosphorus and fluorine in PG. For the dosage of curing agent of 3.0% in the presence of the curing temperature of 30 °C for 150 min, the curing rate of water-soluble phosphorus in PG is obtained as 98.5%, whereas the curing rate of water-soluble fluorine impurities reaches more than 99.0%. After the curing process, PG exhibits good environmental friendliness. The main product of water-soluble fluoride in PG is $CaF_2$ precipitation when using a curing agent for harmless disposal of PG. Therefore, the research in this paper can provide theoretical guidance for the efficient recovery of fluoride resources from PG.

## Author contributions

Conducted all experiments, Wanqiang Dong; designed the experiments and wrote the manuscript, Wanqiang Dong and Ningjie Sun. Funding acquisition, Ru'an Chi and Yuefei Zhang. All authors discussed continuously and contributed to the writing of the manuscript. All authors have read and agreed to the published version of the manuscript.

## Conflicts of interest

There are no conflicts of interest to declare.

## Acknowledgements

This work financially supported by the National Key Research and Development Program Foundation of China (2022YFC3902702), the Chief Scientist Project Foundation of Three Gorges Laboratory (SXCS2204) and Innovation Project of Hubei Three Gorges Laboratory (SC232003).

## References

1 F. Wu, J. Wang, J. Liu, G. Zeng, P. Xiang, P. Hu and W. Xiang, Distribution, geology and development status of phosphate resources, *Geol. China*, 2021, **48**(1), 82–101.
2 S. Rajan and M. P. Upsdell, Environmentally friendly agronomically superior alternatives to chemically processed phosphate fertilizers: Phosphate rock/sulfur/

Acidithiobacillus sp. combinations, *Adv. Agron.*, 2021, **167**, 183–245.

3 N. Sabah, M. Tahir, G. Sarwar, M. Luqman, A. Aziz, M. Manzoor and M. Aftab, Biosolubilization of phosphate rock using organic amendments: An innovative approach for sustainable maize production in Aridisols—A review, *Sarhad J. Agric.*, 2022, **38**, 617–625.

4 R. El Bamiki, O. Raji, M. Ouabid, A. Elghali, O. Khadiri Yazami and J.-L. Bodinier, Phosphate rocks: A review of sedimentary and igneous occurrences in Morocco, *Minerals*, 2021, **11**(10), 1137.

5 B. Li, P. Li, X. C. Zeng, W. Yu, Y. F. Huang, G. Q. Wang and B. R. Young, Assessing the sustainability of phosphorus use in China: Flow patterns from 1980 to 2015, *Sci. Total Environ.*, 2020, **704**, 135305.

6 X. Liu, Z. Yuan, X. Liu, Y. Zhang, H. Hua and S. Jiang, Historic trends and future prospects of waste generation and recycling in China's phosphorus cycle, *Environ. Sci. Technol.*, 2020, **54**(8), 5131–5139.

7 A. R. Jupp, S. Beijer, G. C. Narain, W. Schipper and J. C. Slootweg, Phosphorus recovery and recycling–closing the loop, *Chem. Soc. Rev.*, 2021, **50**(1), 87–101.

8 R. L. Mikkelsen, C. R. Binder, E. Frossard, F. S. Brand, R. W. Scholz, U. Vilsmaier, J. J. Elser, R. Schnee, H. C. Stevens and M. Vermeulen, Use: What is needed to support sustainability?, In *Sustainable Phosphorus Management: A Global Transdisciplinary Roadmap*, Springer, 2014; pp pp 207–246.

9 I. Soboleva and S. Lyashenko, Studying the Hemihydrate Stage of the Process of Preparation of Extractive Phosphoric Acid by the Dihydrate–Hemihydrate Method from Low-Grade Phosphorites, *Theor. Found. Chem. Eng.*, 2023, **57**(4), 704–708.

10 I. Soboleva and E. Koltsova, Investigation of reaction kinetics for industrial dihydrate method of $P_2O_5$ production, In *CHISA 2006-17th International Congress of Chemical and Process Engineering*, 2006.

11 H. Chanouri, K. Agayr, E. M. Mounir, R. Benhida and K. Khaless, Staged purification of phosphogypsum using pH-dependent separation process, *Environ. Sci. Pollut. Res.*, 2024, **31**(7), 9920–9934.

12 B. Li, Z. Liu and C. Tao, *Green Manufacturing of Wet-Process Phosphoric Acid; Chongqing University Electronic Audio and Video*, Publishing House Co., Ltd, 2019.

13 Y. Peifa, C. Junmin and C. Zhihua, Comparison of WPA production technology in China, *Phosphate Compd. Fert.*, 2020, **35**(1), 24–26.

14 D. Wanqiang, D. Xiangyi, Z. Qiutong, S. Shuyang, W. Kang and C. R. an, Effect of Calcium Oxide on Solidification Properties of Soluble Phosphorus and Soluble Fluorine in Phosphogypsum, *J. Wuhan Inst. Technol.*, 2023, **45**(6), 620–627.

15 Y. Shi, X. Wang, Z. Qing, Y. Song, J. Min, Y. Zhou, J. Du and S. Wang, Using Iron Tailings for Phosphate Removal in Cemented Phosphogypsum (PG) Backfill, *Materials*, 2022, **15**(23), 8497.

16 Q.-s. Chen, S.-y. Sun, Y.-k. Liu, C.-c. Qi, H.-b. Zhou and Q.-l. Zhang, Immobilization and leaching characteristics of fluoride from phosphogypsum-based cemented paste backfill, *Int. J. Miner., Metall. Mater.*, 2021, **28**(9), 1440–1452.

17 Z. Wei and Z. Deng, Research hotspots and trends of comprehensive utilization of phosphogypsum: Bibliometric analysis, *J. Environ. Radioact.*, 2022, **242**, 106778.

18 X. Qin, Y. Cao, H. Guan, Q. Hu, Z. Liu, J. Xu, B. Hu, Z. Zhang and R. Luo, Resource utilization and development of phosphogypsum-based materials in civil engineering, *J. Cleaner Prod.*, 2023, **387**, 135858.

19 J. Yang, M. Li, L. Liu, H. Zhao, W. Luo, Y. Guo, X. Ji and W. Hu, Dynamic characteristics of net anthropogenic phosphorus input to the upper Yangtze River Basin from 1989 to 2019: Focus on the phosphate ore rich area in China, *J. Environ. Manage.*, 2023, **347**, 119140.

20 Y. Cui, J. Bai, I.-S. Chang and J. Wu, A systematic review of phosphogypsum recycling industry based on the survey data in China–applications, drivers, obstacles, and solutions, *Environ. Impact Assess. Rev.*, 2024, **105**, 107405.

21 L. Hao and Q. Zunwen, Challenges and Countermeasures for Comprehensive Utilization of Phosphogypsum in Hubei Province, *Technology and Economy of Changjiang*, 2023, **7**(5), 102–106.

22 F. Akfas, A. Elghali, A. Aboulaich, M. Munoz, M. Benzaazoua and J.-L. Bodinier, Exploring the potential reuse of PG: A waste or a resource?, *Sci. Total Environ.*, 2023, 168196.

23 J. Qi, H. Zhu, P. Zhou, X. Wang, Z. Wang, S. Yang, D. Yang and B. Li, Application of phosphogypsum in soilization: a review, *Int. J. Environ. Sci. Technol.*, 2023, **20**(9), 10449–10464.

24 Y. Chernysh, O. Yakhnenko, V. Chubur and H. Roubík, Phosphogypsum recycling: a review of environmental issues, current trends, and prospects, *Appl. Sci.*, 2021, **11**(4), 1575.

25 Y. Chen, J. V. García-Meza, B. Zhou, Z. Peng, Q. Chen, R. M. Kasomo, X. Weng, H. Li and S. Song, Efficient recovery of fluorine from wet-process phosphoric acid using silicon powder as a new and eco-friendly reagent, *Sep. Purif. Technol.*, 2024, **337**, 126435.

26 M. F. Cheira, M. Rashed, A. Mohamed, G. Hussein and M. Awadallah, Removal of some harmful metal ions from wet-process phosphoric acid using murexide-reinforced activated bentonite, *Mater. Today Chem.*, 2019, **14**, 100176.

27 Y. Zhou, G. Zheng, Y. Long, Z. Liu, C. Tao and R. Liu, Advanced oxidation processes for wet-process phosphoric acid: Enhanced phosphorus recovery and removal of organic matters, *Hydrometallurgy*, 2022, **210**, 105842.

28 G. Steiner, B. Geissler, I. Watson and M. C. Mew, Efficiency developments in phosphate rock mining over the last three decades, *Resour., Conserv. Recycl.*, 2015, **105**, 235–245.

29 J. Xiang, J. Qiu, Y. Song, Y. Miao and X. Gu, Synergistic removal of phosphorus and fluorine impurities in phosphogypsum by enzyme-induced modified microbially induced carbonate precipitation method, *J. Environ. Manage.*, 2022, **324**, 116300.

30 X. Lv and L. Xiang, The generation process, impurity removal and high-value utilization of phosphogypsum material, *Nanomaterials*, 2022, **12**(17), 3021.
31 Z. Hongtao, B. Weijun, S. Zhenhua, L. Songgeng, L. Huiquan and L. Weigang, Deep removal of impurities from phosphogypsum, *Chem. Ind. Eng. Prog.*, 2017, **36**(4), 1240.
32 M. Wang, X. Yuan, W. Dong, Q. Fu, X. Ao and Q. Chen, Gradient removal of Si and P impurities from phosphogypsum and preparation of anhydrous calcium sulfate, *J. Environ. Chem. Eng.*, 2023, **11**(3), 110312.
33 W. Zhang, L. Zhao, M. Xue, X. Duan, C. Feng and J. Zhu, Efficient precipitation of soluble phosphorus impurities in the recycling of phosphogypsum to produce hemihydrate gypsum, *J. Cleaner Prod.*, 2023, **396**, 136455.
34 M. Karibayev, B. Myrzakhmetov, S. Kalybekkyzy, Y. Wang and A. Mentbayeva, Binding and degradation reaction of hydroxide ions with several quaternary ammonium head groups of anion exchange membranes investigated by the DFT method, *Molecules*, 2022, **27**(9), 2686.
35 H.-M. Liu, X.-J. Zhao, Y.-Q. Zhu and H. Yan, DFT study on MgAl-layered double hydroxides with different interlayer anions: structure, anion exchange, host–guest interaction and basic sites, *Phys. Chem. Chem. Phys.*, 2020, **22**(4), 2521–2529.
36 L. Tonghai, *Study on the Crystallization Process of Calcium Sulfate Dihydrate in the Wet Process Phosphoric Acid System*, Hefei University of Technology, Hefei, Anhui, P.R. China, 2016.
37 Y. Ennaciri and M. Bettach, The chemical behavior of the different impurities present in Phosphogypsum: a review, *Phosphorus, Sulfur Silicon Relat. Elem.*, 2024, **199**(2), 129–148.
38 A. M. Borst, M. P. Smith, A. A. Finch, G. Estrade, C. Villanova-de-Benavent, P. Nason, E. Marquis, N. J. Horsburgh, K. M. Goodenough and C. Xu, Adsorption of rare earth elements in regolith-hosted clay deposits, *Nat. Commun.*, 2020, **11**(1), 4386.
39 K. L. Walz Mitra, C. H. Chang, M. P. Hanrahan, J. Yang, D. Tofan, W. M. Holden, N. Govind, G. T. Seidler, A. J. Rossini and A. Velian, Surface functionalization of black phosphorus with nitrenes: identification of P= N bonds by using isotopic labeling, *Angew. Chem.*, 2021, **133**(16), 9209–9216.
40 L. Ji, Y. Wei, P. Wu, M. Xu, T. Wang, S. Wang, Q. Liang, T. J. Meyer and Z. Chen, Heterointerface engineering of Ni2P–Co2P nanoframes for efficient water splitting, *Chem. Mater.*, 2021, **33**(23), 9165–9173.
41 K. S. Siow, L. Britcher, S. Kumar and H. J. Griesser, XPS study of sulfur and phosphorus compounds with different oxidation states, *Sains Malays.*, 2018, **47**(8), 1913–1922.
42 A. Kazragis, High-temperature decontamination and utilization of phosphogypsum, *J. Environ. Eng. Landsc. Manag.*, 2004, **12**(4), 138–145.
43 Y. Chu, M. A. Khan, M. Xia, W. Lei, F. Wang and S. Zhu, Synthesis and mechanism of adsorption capacity of modified montmorillonite with amino acids for 4-acetaminophenol removal from wastewaters, *J. Chem. Eng. Data*, 2019, **64**(12), 5900–5909.
44 Y. Chu, S. Zhu, F. Wang, W. Lei, M. Xia and C. Liao, Tyrosine-immobilized montmorillonite: an efficient adsorbent for removal of $Pb^{2+}$ and $Cu^{2+}$ from aqueous solution, *J. Chem. Eng. Data*, 2019, **64**(8), 3535–3546.